

Visual Language Maps for Robot Navigation

Chenguang Huang¹, Oier Mees¹, Andy Zeng², Wolfram Burgard³

Abstract—Grounding language to the visual observations of a navigating agent can be performed using off-the-shelf visual-language models pretrained on Internet-scale data (e.g., image captions). While this is useful for matching images to natural language descriptions of object goals, it remains disjoint from the process of mapping the environment, so that it lacks the spatial precision of classic geometric maps. To address this problem, we propose VLMaps, a spatial map representation that directly fuses pretrained visual-language features with a 3D reconstruction of the physical world. VLMaps can be autonomously built from video feed on robots using standard exploration approaches and enables *natural language indexing of the map* without additional labeled data. Specifically, when combined with large language models (LLMs), VLMaps can be used to (i) translate natural language commands into a sequence of open-vocabulary navigation goals (which, beyond prior work, can be spatial by construction, e.g., “in between the sofa and TV” or “three meters to the right of the chair”) directly localized in the map, and (ii) can be shared among multiple robots with different embodiments to generate new obstacle maps on-the-fly (by using a list of obstacle categories). Extensive experiments carried out in simulated and real world environments show that VLMaps enable navigation according to more complex language instructions than existing methods. Videos are available at <https://vlmaps.github.io>.

I. INTRODUCTION

People are excellent navigators of the physical world – due in part to our remarkable ability to build cognitive maps [1] that form the basis of spatial memory [2], [3] to (i) localize landmarks at varying ontological levels, such as a book; on the shelf; in the living room, or (ii) determine whether the layout permits navigation between two points. Classic methods for robot navigation [4], [5] build geometric maps for path planning, which can parse goals from natural language commands [6], [7], but struggle to generalize to unseen instructions. Learning methods directly optimize for navigation policies grounded in language end-to-end (commands to actions) [8], [9], but require copious amounts of data collection.

Meanwhile, recent works show that visual-language models (VLMs) [10], [11] pretrained on Internet-scale data (e.g., image captions) can be used out-of-the-box to ground language to the visual observations of a navigating agent, without additional data collection or model finetuning. These models enable mobile robots to handle new instructions that specify unseen object goals, and can be combined with exploration algorithms to search for the first instance of any object (CoW) [12], or traverse object-centric landmarks in graphs (LM-Nav) [13]. While promising, these methods predominantly use VLMs as critics to match image observations to object goal descriptions, but do so in ways that remain disjoint from the mapping of the environment. Without grounding language onto a spatial representation, these systems

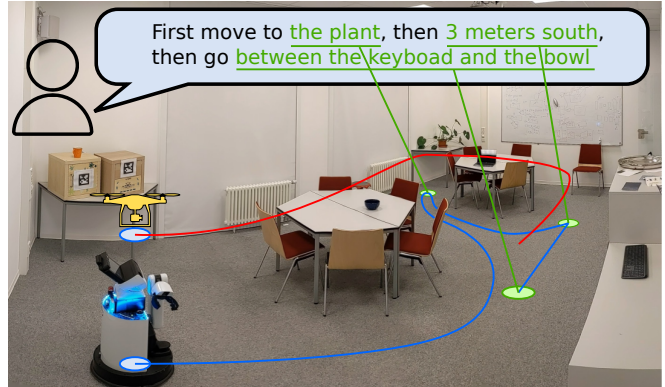


Fig. 1: **VLMaps** is a spatial map representation in which pretrained visual-language model features are fused into a 3D reconstruction of the physical world. Spatially anchoring visual language features enables *natural language indexing in the map*, which can be used to e.g., localize landmarks or spatial references with respect to landmarks – enabling zero-shot spatial goal navigation without additional data collection or model finetuning.

may struggle to (i) recognize correspondences that associate independent observations of the same object, (ii) localize spatial goals e.g., “in between the sofa and TV”, or (iii) build persistent representations that can be shared across different embodiments e.g., mobile robots, drones. Existing VLM-based solutions generalize to new object goals, but lose the spatial precision of classic geometric maps – is it possible to get the best of both?

In this work, we investigate the utility of a *spatial* visual-language map representation VLMaps, wherein pretrained visual-language features from image observations are directly fused into a 3D reconstruction of the physical world. These representations can be autonomously built from video feed on robots using standard exploration algorithms. When paired with large language models (LLMs) in Socratic fashion [14], VLMaps can translate natural language instructions into a sequence of open-vocabulary goals, directly localized in the map. A key aspect of VLMaps is that it is spatial, which enables it to:

- Localize spatial goals beyond object-centric ones, e.g., “in between the TV and sofa” or “to the right of the chair” or “kitchen area” using code-writing LLMs, expanding beyond capabilities of CoW or LM-Nav.
- Generate new obstacle maps for new embodiments given natural language descriptions of landmark categories that they can or cannot traverse e.g., “tables” are obstacles for a large mobile robot, but traversable for a drone.

Extensive experiments show that using VLMaps enables more effective long-horizon multi-object goal navigation than baseline alternatives, e.g., CoW [12] and LM-Nav [13], and in particular, excels at enabling spatial open-vocabulary navigation tasks. We also provide ablations on different ways of constructing

¹University of Freiburg, Germany.

²Google Research, USA.

³University of Technology Nuremberg, Germany.

This work has been supported partly by the German Federal Ministry of Education and Research under contract 01IS18040B-OML



Fig. 2: VLMaps enables a robot to perform complex zero-shot spatial goal navigation tasks given natural language commands, without additional data collection or model finetuning.

VLMaps with different language models, as well as a discussion on limitations, which point to areas for future work. Code and videos are available at <https://vlmaps.github.io>.

II. RELATED WORK

Semantic Mapping. The maturity of traditional SLAM techniques together with the advancements in semantic understanding capabilities of convolutional neural networks has recently spurred considerable interest around augmenting 3D maps with semantic information [15], [16]. The literature has focused on either densely annotating 3D volumetric maps with 2D semantic segmentation CNNs [16] or object-oriented approaches [17], [18], [19], which build 3D maps around detected objects to enable object-level pose graph optimization. Although, progress has been made at generating more abstract maps, such as scene graphs [20], [21], current approaches are limited to a predefined set of semantic classes. In contrast, VLMaps builds an open-vocabulary semantic map that unlike prior work enables *natural language indexing in the map*.

Vision & Language Navigation. Vision-and-Language Navigation (VLN) has recently attracted increasing amount of attention from the community [8], [22]. Earlier work has focused on learning end-to-end policies that can follow route-based instructions on topological graphs of simulated environments [8], [23], [24]. However, agents trained in this setting do not have low-level planning capabilities and rely heavily on the topological graph, limiting their real world applicability [9]. Moreover, despite extensions to continuous state spaces [22], [25], [26], most of these learning-based methods are data-intensive.

Zero-shot Models. The recent success of large pretrained vision and language models [10], [27] has spurred a flurry of interest in applying their zero-shot capabilities to domains ranging from object detection and segmentation [28], [29], [11], robot manipulation [30], [31], [32], [33] to navigation [13], [12], [34]. Most related to our work, LM-Nav [13] combines three pre-trained models to navigate via a topological graph in the real world. CoW [12] performs zero-shot language-based object navigation by combining CLIP-based [10] saliency maps and traditional exploration methods. However, both LM-Nav [13] and CoW [12] are limited to navigating to object landmarks, failing to understand finer-grained queries, such as “to the left of the chair” and “in between the TV and sofa”. In contrast, our method enables spatial language indexing beyond object-centric goals, and can generate open-vocabulary obstacle maps. Concurrent work, NLMap [34] shows that VLMs can be used to build queryable scene representations to allow LLM robot planning [35] with new objects and locations.

III. METHOD

Our goal is to build a *spatial* visual-language map representation, in which landmarks (“the sofa”) or spatial references (“between the sofa and TV”) can be directly localized using natural language. We propose VLMaps as one such representation, which can be constructed using off-the-shelf visual-language models (VLMs) and standard 3D reconstruction libraries. In the following subsections, we describe (i) how to build a VLMap (Sec. III-A), (ii) how to use these maps to localize open-vocabulary landmarks (Sec. III-B), (iii) how to build open-vocabulary obstacle maps from a list of obstacle categories for different robot embodiments (Sec. III-C), and (iv) how VLMaps can be used together with large language models (LLMs) for zero-shot spatial goal navigation on real robots from natural language commands (Sec. III-D), without additional data collection or model finetuning. Our pipeline is visualized in Fig. 3.

A. Building a Visual-Language Map

The key idea behind building a VLMap is to fuse pretrained visual-language features into a 3D reconstruction. This can be done by computing dense pixel-level embeddings from an existing visual-language model (over the video feed of the robot) and back-projecting them onto the 3D surface of the environment (captured from depth data used for reconstruction with visual odometry).

In our work, we utilize LSeg [11] as the visual-language model, a language-driven semantic segmentation model which segments the RGB images based on a set of free-form language categories. The LSeg visual encoder maps an image such that each pixel’s embedding lies in CLIP features space. In our approach, the LSeg pixel embeddings are fused into their corresponding 3D map locations. In this way, without explicit manual segmentation labels, we incorporate a powerful language-driven semantic prior that inherits the generalization capabilities of VLMs. The only assumption our method makes is access to odometry, to enable building a map from sequences of RGB-D images, which is readily available from RGB-D SLAM systems.

Formally, we define VLMap as $\mathcal{M} \in \mathbb{R}^{\bar{H} \times \bar{W} \times C}$, where \bar{H} and \bar{W} represent the size of the top-down grid map, and C represents the length of the VLM embedding vector for each grid cell. Together with the scale parameter s , a VLMap \mathcal{M} represents an area with size $s\bar{H} \times s\bar{W}$ meters. In order to build the map, for each RGB-D frame we first back-project all the depth pixels $\mathbf{u} = (u, v)$ to form a local depth point cloud and transform it to the world frame, $\mathbf{P}_k = D(\mathbf{u})K^{-1}\tilde{\mathbf{u}}$ and $\mathbf{P}_W = T_{Wk}\mathbf{P}_k$ where $\tilde{\mathbf{u}} = (u, v, 1)$, K is the intrinsic matrix of the depth camera, $D(\mathbf{u}) \in \mathbb{R}$ is the depth value of the pixel \mathbf{u} , T_{Wk} is the transformation from the world coordinate frame to the k -th camera frame, $\mathbf{P}_k \in \mathbb{R}^3$ is

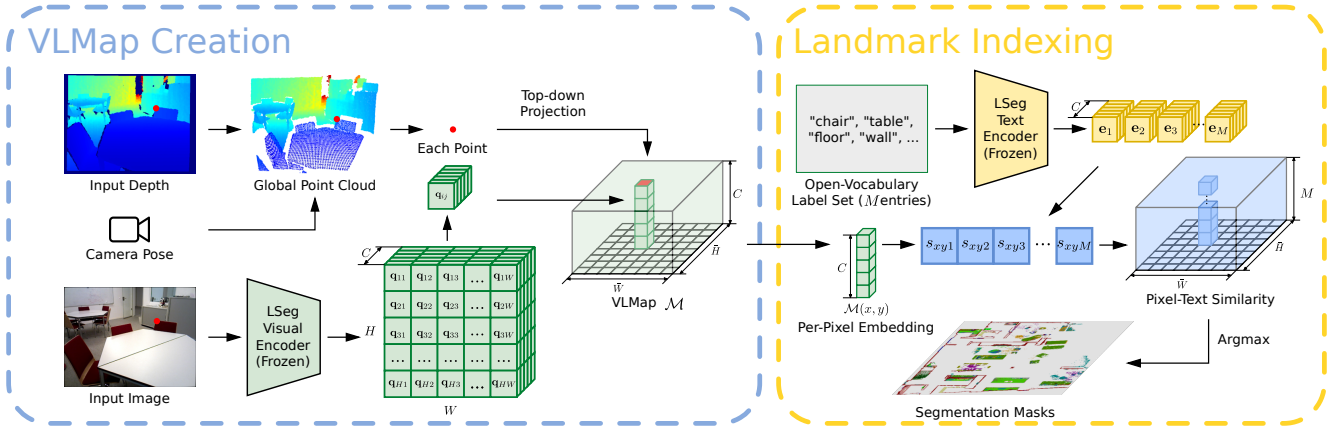


Fig. 3: System overview. A VLM is created by fusing pretrained visual-language features into the reconstruction of the environment to enable visual-spatial-language-based reasoning. By providing a list of open-vocabulary labels, segmentation masks for corresponding semantic classes are retrieved for downstream applications.

the 3D point position in the k -th frame, and $\mathbf{P}_W \in \mathbb{R}^3$ is the 3D point position in the world coordinate frame. We then project the point \mathbf{P}_W to the ground plane and get the pixel \mathbf{u} 's corresponding position on the grid map,

$$p_{map}^x = \left\lfloor \frac{\bar{H}}{2} + \frac{P_W^x}{s} + 0.5 \right\rfloor, p_{map}^y = \left\lfloor \frac{\bar{W}}{2} - \frac{P_W^z}{s} + 0.5 \right\rfloor \quad (1)$$

where p_{map}^x and p_{map}^y represent the coordinates of the projected point in the map \mathcal{M} .

Once the grid map is built, we apply LSeg's visual encoder $f(\mathcal{I}) : \mathbb{R}^{H \times W \times 3} \rightarrow \mathbb{R}^{H \times W \times C}$ to the RGB image \mathcal{I}_k and generate the pixel-level embedding $\mathcal{F}_k \in \mathbb{R}^{H \times W \times C}$. Given the RGB-D registration, we project each image pixel \mathbf{u} 's embedding $\mathbf{q} = \mathcal{F}_k(\mathbf{u}) \in \mathbb{R}^C$ to its corresponding grid cell location (p_{map}^x, p_{map}^y) in the top-down grid map. Intuitively, there exist multiple 3D points projecting to the same grid location in the map. Thus, we average their embeddings, $\mathcal{M}(p_{map}^x, p_{map}^y) = \frac{1}{n} \sum_{i=1}^n \mathbf{q}_i$ where $\mathcal{M}(p_{map}^x, p_{map}^y) \in \mathbb{R}^C$ represents the map features at the grid position (p_{map}^x, p_{map}^y) , n represents the total number of points projecting to the grid location (p_{map}^x, p_{map}^y) , and $\mathbf{q}_i \in \mathbb{R}^C$ denotes each point's corresponding pixel embedding. We note that these n points might not only come from a single frame, but also from points from multiple frames. Therefore, the resulting features contain the averaged embeddings from multiple views of the same object.

B. Localizing Open-Vocabulary Landmarks

We now describe how to localize landmarks in VLMs with free-form natural language. Formally, we define the input language list as $\mathcal{L} = [\mathbf{l}_0, \mathbf{l}_1, \dots, \mathbf{l}_M]$ where \mathbf{l}_i represents the i -th category in text form, and M represents the number of categories defined by the user. Some examples of the input language list are ["chair", "sofa", "table", "other"] or ["furniture", "floor", "other"]. As Li *et al.* [11], we apply the pre-trained CLIP text encoder [10] to convert such list of texts into a list of vector embeddings $[\mathbf{e}_0, \mathbf{e}_1, \dots, \mathbf{e}_M]$, $\mathbf{e} \in \mathbb{R}^C$, which are organized into an embedding matrix $E \in \mathbb{R}^{M \times C}$, where each row of the matrix represents the embedding of a category. The map embeddings \mathcal{M} are also flattened into a matrix $Q \in \mathbb{R}^{\bar{H}\bar{W} \times C}$, where each row represents the embedding of a pixel in the top-down grid map. We then compute the pixel-to-category

similarity matrix $S = Q \cdot E^T$, where $S \in \mathbb{R}^{\bar{H}\bar{W} \times M}$. Each element S_{ij} in the matrix stores the similarity value between a pixel and a text category, indicating how likely this pixel belongs to the class. By applying the argmax operator along the row direction to S and reshaping the resulting vector to shape $\bar{H} \times \bar{W}$, we get the final segmentation result $R \in \mathbb{R}^{\bar{H} \times \bar{W}}$. Each element R_{ij} represents the label index of the input language list \mathcal{L} at the grid map location (i, j) . With the final resulting matrix R , we compute the most related language-based category for every pixel in the grid map.

C. Generating Open-Vocabulary Obstacle Maps

Building a VLM enables us to generate obstacle maps that inherit the open-vocabulary nature of the VLMs used (LSeg and CLIP). Specifically, given a list of obstacle categories described with natural language, we can localize those obstacles at runtime to generate a binary map for collision avoidance and/or shortest path planning. A prominent use case for this is sharing a VLM of the same environment between different robots with different embodiments (i.e., cross-embodiment problem [36], [37]), which may be useful for multi-agent coordination [38]. For example, a large mobile robot may need to navigate around a table (or other large furniture), while a drone can directly fly over it. By simply providing two different lists of obstacle categories – one for the large mobile robot (that contains "table"), and another for the drone (that does not), we can generate two distinct obstacles maps for the two robots to use respectively, sourced on-the-fly from the same VLM.

To do so, we first extract an obstacle map $\mathcal{O} \in \{0, 1\}^{\bar{H} \times \bar{W}}$ where each projected position of the depth point cloud in the top-down map is assigned 1, and otherwise 0. To avoid points from the floor or the ceiling, points P_W are filtered out depending on their height,

$$\mathcal{O}_{ij} = \begin{cases} 1, & t_1 \leq P_W^y \leq t_2 \text{ and } p_{map}^x = i \text{ and } p_{map}^y = j \\ 0, & \text{otherwise} \end{cases} \quad (2)$$

where $t_1, t_2 \in \mathbb{R}$ are the lower and upper thresholds for the y component of the point P_W . Second, to obtain obstacle maps tailored to a certain embodiment, we define a list of potential obstacle categories $\mathcal{L}_{obs} = [\mathbf{l}_{obs0}, \mathbf{l}_{obs1}, \dots, \mathbf{l}_{obsM}]$, where \mathbf{l}_i represents the i -th obstacle category in language, and M

represents the total number of obstacle categories defined by the user. We then apply the open-vocabulary landmark indexing introduced in III-B and obtain segmentation masks for all defined obstacles. For a specific embodiment k , we choose a subset of classes out of the whole potential obstacle list \mathcal{L}_{obs} and take union of their segmentation masks to get the obstacles mask $\tilde{\mathcal{O}}_{em_k}$. We ignore false predictions of obstacles on floor region in $\tilde{\mathcal{O}}_{em_k}$ by taking intersection with \mathcal{O} to get the final obstacles map \mathcal{O}_{em_k} .

D. Zero-Shot Spatial Goal Navigation from Language

In this section, we describe our approach to long-horizon (spatial) goal navigation, given a set of landmark descriptions specified by natural language instructions, for example:

```
move first to the left side of the counter, then
move between the sink and the oven, then move back
and forth to the sofa and the table twice
```

Notably different from prior work [12], [13], our approach with VLMs allows referencing precise spatial goals such as: “in between the sofa at the TV” or “3 meters east of the chair.” Specifically, we use a large language model (LLM) to interpret the input natural language commands and break them down into subgoals [35], [13], [14]. But in contrast to prior work, which may reference these subgoals with language and map to low-level policies with semantic translation [39] or affordances [35], [40], [41], [42], we leverage the code-writing capabilities of LLMs to generate executable Python robot code [43], [33], [44], [27] that can (i) make precise calls to parameterized navigation primitives, and (ii) perform arithmetic when needed. The generated code can simply be executed on the system with the built-in Python `exec` function.

Note that recent works [43], [33], [44], [27] have shown that code-writing language models (e.g., Codex [44]) trained on billions of lines of code from Github can be used to synthesize new simple Python programs from docstrings. In this work, we repurpose these models for mobile robot planning, by priming them with several input examples of natural language commands (formatted as comments) paired with corresponding robot code (via few-shot prompting). Robot code can express functions or logic structures (if/else statements, for/while loops) and parameterize API calls (e.g., `robot.move_to(target_name)` or `robot.turn(degrees)`, full list in Appendix Sec. A) that map to spatial behaviors specified by the language commands. At test time, the models can subsequently take in new commands and autonomously re-compose API calls to generate new robot code respectively (prompt in gray, input task commands in green, and generated outputs are highlighted):

```
# move a bit to the right of the fridge
robot.move_to_right('refrigerator')
# face the toilet
robot.face('toilet')
# move to the west of the chair
robot.move_west('chair')
# turn right 20 degrees
robot.turn(20)
# move back and forth to the chair and table 3 times
pos1 = robot.get_pos('chair')
...
# move forward for 3 meters
robot.move_forward(3)
```

```
# move first to the left side of the counter, then
move between the sink and the oven, then move back and
forth to the sofa and the table twice
robot.move_to_left('counter')
robot.move_in_between('sink', 'oven')
pos1 = robot.get_pos('sofa')
pos2 = robot.get_pos('table')
for i in range(2):
    robot.move_to(pos1)
    robot.move_to(pos2)
# move 2 meters north of the laptop, then move 3
meters rightward
robot.move_north('laptop')
robot.face('laptop')
robot.turn(180)
robot.move_forward(2)
robot.turn(90)
robot.move_forward(3)
```

The code-writing LLM generates code that not only references the new landmarks mentioned in the language commands (as comments), but also can chain together new sequences of API calls to follow unseen instructions accordingly. The prompt has been truncated here for brevity, see the full prompt in Appendix Sec. B.

The navigation primitive functions being called by the language model (e.g., `robot.move_to_left('counter')`) use a pre-generated VLM to localize the coordinates of the open-vocabulary landmarks ('counter') in the maps (described in Sec. III-B) modified with predefined scripted offsets (to define “left”). We then navigate to these coordinates using an off-the-shelf navigation stack that takes as input the embodiment-specific obstacle map (generated using the same VLM, with the process described in Sec. III-C).

IV. EXPERIMENTS

The goal of our experiments are four-fold: (i) to quantitatively evaluate our method with VLMs against recent open-vocabulary navigation baselines on the standard task of multi-object goal navigation (Sec. IV-B), (ii) to investigate whether our method can better navigate to *spatial* goals specified by language commands versus alternative approaches (Sec. IV-C), (iii) to study whether VLMs and their capacity to specify open-vocabulary obstacle maps can provide utility in improving the navigation efficiency of different robots with different embodiments (Sec. IV-D), and (iv) to demonstrate on real robots that VLMs can enable zero-shot spatial goal navigation given unseen language instructions (Sec. IV-E).

A. Simulation Setup

Experimental setup. We use the Habitat simulator [45] with the Matterport3D dataset [46] for evaluation of multi-object navigation and spatial goals navigation tasks. The dataset contains a large set of realistic indoor scenes that help evaluate the generalization capabilities of navigation agents. To evaluate open-vocabulary multi-embodiment obstacle maps creation, we adopt the AI2THOR simulator due to its support of multiple agent types, such as LoCoBot and drone. In these two environments, the robot is required to navigate in a continuous environment with actions: **move forward 0.05 meters, turn left 1 degree, turn right 1 degree** and **stop**. For map creation in Habitat, we collect 12,096 RGB-D frames across ten different scenes and record the

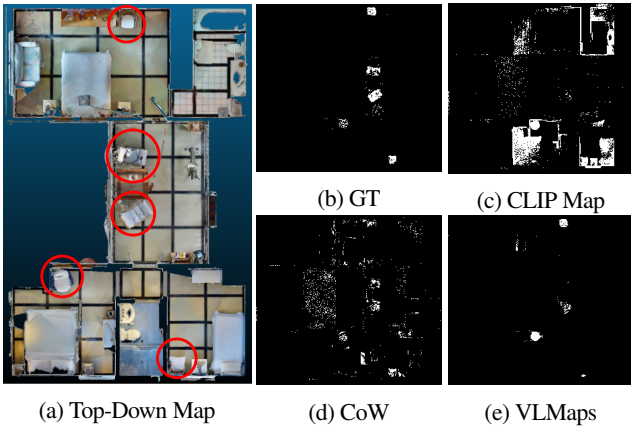


Fig. 4: Object mask for object type “chair”. 4a shows the top-down map of the scene and the red circles specify the locations of type “chair”. 4b shows the ground truth mask for type “chair” and 4c, 4d, 4e show the predicted masks by CLIP Map, CoW and VLMaps.

camera pose of each frame. Similarly, we collect 1,826 RGB-D frames across ten rooms in AI2THOR.

Baselines. We evaluate our method (VLMaps) against 3 baseline methods, all of which utilize visual-language models and are capable of zero-shot language-based navigation:

- LM-Nav [13] creates a graph where image observations of an environment are stored as nodes while the proximity between images are represented as edges. By combining GPT-3 and CLIP, it parses language instructions into a list of landmarks and plans on the graph towards corresponding nodes.
- CLIP on Wheels (CoW) [12] achieves language-based object navigation by building a saliency map for the target category with CLIP and GradCAM [47]. By thresholding the saliency values, it retrieves a segmentation mask for the target object category and then plans the path on the map.
- CLIP-features-based map (CLIP Map) is an ablative baseline that generates a feature map for the environment in a similar way as ours. Instead of using LSeg visual features, it projects the CLIP visual features onto the map averaged across views. Object category masks are generated by thresholding the similarity between map features and the object category features.

For additional context and analysis, we also report results from a system that has access to a ground truth semantic map for navigation, to provide a systems-level upper bound on performance.

B. Multi-Object Navigation

We collect 91 sequences of tasks for the evaluation of object navigation. In each sequence, we randomly specify a starting position of the robot in one scene and then pick 4 among 30 object categories as subgoal object types. The robot is required to navigate to these 4 subgoals sequentially. In each sequence of subgoals, when the robot reaches one subgoal category, it should call the **stop** action to indicate its progress. We consider the navigation to one subgoal as success when the stop position’s distance to the correct object is within 1 meter. In order to evaluate the long-horizon navigation capabilities of the agents, we compute the Success Rate (SR) of continuously reaching 1 to 4 subgoals in a sequence, shown in Tab. I. We also report the independent

subgoal success rate, which indicates the total successful subgoals number divided by the total subgoals number (364 subgoals).

Tasks	No. Subgoals in a Row				Independent Subgoals
	1	2	3	4	
LM-Nav [13]	26	4	1	1	26
CoW [12]	42	15	7	3	36
CLIP Map	33	8	2	0	30
VLMaps (ours)	59	34	22	15	59
GT Map	91	78	71	67	85

TABLE I: Our method (VLMaps) performs favorably over alternative open-vocabulary baselines on multi-object navigation (success rate %), and specifically excels on longer-horizon tasks with multiple sub-goals.

We observe that VLMaps performs consistently better compared to all baselines. LM-Nav has a weak performance as it is only able to navigate to locations represented by images stored in graph nodes. In order to get more insights behind the map-based methods, we visualize the object masks generated by VLMaps, CoW, and CLIP Map, in comparison to GT, in Figure 4. The masks generated by CoW (Figure 4d) and CLIP (Figure 4c) both contain considerable false positive predictions. Since the planning plans the path to the nearest masked target area, these predictions lead to planning towards wrong goals. In contrast, VLMaps’ predictions (Figure 4e) are less noisy, which leads to higher success rates in object navigation.

C. Zero-Shot Spatial Goal Navigation from Language

In these experiments, we investigate the performance of VLMaps versus other baselines for zero-shot *spatial* goal navigation from language. Our benchmark consists of 21 trajectories in 7 scenes, with manually specified corresponding language instructions for evaluation. Each trajectory contains 4 different spatial locations as subgoals. Examples of subgoals are “east of the table”, “in between the chair and the sofa”, or “move forward 3 meters”. There are also instructions for the robot to realign itself in reference to nearby objects such as “with the counter on your right”. Only when the robot reaches the subgoal location within a range of 1 meter can the subgoal be considered to have been reached successfully. We compute the in-a-row success rate in the same way as in Sec. IV-B. For all map-based methods, including CoW, CLIP Map, ground truth semantic map and our method, we apply the code generation techniques introduced in III-D. For LM-Nav, we simply use the same parsing method in the original paper [13] to break down the language instruction into subgoals.

Tasks	No. Subgoals in a Row			
	1	2	3	4
LM-Nav [13]	5	5	0	0
CoW [12]	33	5	0	0
CLIP Map	19	0	0	0
VLMaps (ours)	62	33	14	10
GT Map	76	48	33	29

TABLE II: VLMaps can be used to navigate to spatial goals specified by natural language, and substantially outperforms other open-vocabulary zero-shot navigation baseline alternatives (success rate %) in this setting.

Table II summarizes the zero-shot spatial goal navigation success rates. Our method outperforms other baselines in this task.

Different from object navigation tasks where agents only need to approach a certain object type within a range disregarding the relative spatial shift to the object, the language-based spatial goal navigation tasks require the robot to accurately arrive at the described location in reference to the object. This poses a bigger challenge to the landmark localization ability of the method. The low localization ability of CoW and CLIP Map analyzed in the previous section IV-B leads to their high failure rates in this task.

D. Cross-Embodiment Navigation

We study VLMaps’ ability to improve navigation efficiency by retrieving different obstacle maps for navigation with different embodiments (given the same VLMMap). We evaluate over 100 sequences of subgoals as in Sec. IV-B in AI2THOR simulator. We evaluate VLMaps on both a LoCoBot and a drone to test its capability of generating obstacle maps at runtime for multi-embodiment navigation. We apply the open-vocabulary obstacle map generation method in Sec. III-C to create an obstacle map for the drone (drone map) and one for the LoCoBot (ground map) by defining obstacles for them differently (see the prompts in Appendix Sec. E). We test the navigation ability of these embodiments with three setups: a LoCoBot with a ground map, a drone with a ground map, and a drone with a drone map.

We evaluate the Success Rate (SR) and the Success rate weighted by the (normalized inverse) Path Length (SPL) [48] defined as: $SPL = \frac{1}{N} \sum_{i=1}^N S_i \frac{l_i}{\max(p_i, l_i)}$ where N is the total number of evaluated tasks, $S_i \in \{0, 1\}$ is the binary indicator of success, l_i denotes the ground truth shortest path length, and p_i denotes the actual path length of the agent in navigation. This metric indicates how efficient the actual path is compared to the ground truth shortest path when the navigation task is success. In our three setups, the ground truth trajectories for the LoCoBot and the drone are planned on floor-level and on 1.7-meter-height-level respectively.

Tasks	No. Subgoals in a Row								Independent Subgoals
	1		2		3		4		
	SR	SPL	SR	SPL	SR	SPL	SR	SPL	SR
LoCoBot (ground map)	53	49.0	28	17.8	14	6.7	6	2.5	52.3
Drone (ground map)	53	41.8	28	15.5	14	5.3	6	2.0	53.3
Drone (drone map)	56	45.4	30	16.3	17	7.0	7	2.5	55.0

TABLE III: VLMaps generates different obstacle maps for different robot embodiments, conditioned on a list of obstacle categories. This improves object navigation efficiency (Success % weighted by Path Length, SPL) of e.g., drones, which can benefit from custom obstacle maps that differ from the ground map (originally for LoCoBot, a large mobile robot).

Results in Tab. III show that the average navigation success rates of the ground-map version of the LoCoBot and the drone are similar because the same obstacles map is used for planning. However, there is an obvious gap between their SPL values. This is because when the drone does not have access to a customized obstacle map, it fails to benefit from flying over ground objects to improve the navigation efficiency. In contrast, while achieving similar success rate compared to the drone with a ground map, the drone with a drone map manages to navigate with higher path efficiency, reflected by the increased SPL values. The comparable SPL values for the drone with the drone map and the LoCoBot with the ground map shows that VLMaps helps to generalize the



Fig. 5: VLMaps enables different embodiments to define their own obstacle maps for navigation. The left image shows the top-down view of an environment. The middle columns show the observations of agents during navigation. The images on the right demonstrate the obstacles maps generated for different embodiments and the corresponding navigation paths.

navigation efficiency among different embodiments. An example of the multi-embodiment object navigation task is shown in Fig. 5, where by defining a more efficient obstacles map, the drone flies over the sofa and reaches the laptop target directly, while the LoCoBot has to move aside first to avoid colliding into the sofa.

E. Real Robot Experiments

We execute real world experiments on the HSR mobile robot for indoor navigation, given natural language commands. For map creation, we record 374 frames for the evaluated scene and use an off-the-shelf RGB-D SLAM solution, RTAB-Map [49], to estimate the camera poses. During inference, we also use RTAB-Map’s global localization module to initialize the robot pose. We test our VLMaps in a semantically rich indoor scene with more than 10 different classes of objects. 20 different language-based spatial goals are defined for testing purpose. Across different test runs, we initialize the robot at different locations.

The robot finishes 10 navigation goals out of the 20. Among the successful trials, six of them are spatial goals like “move between the chair and the wooden box” or “move to the south of the table”. three of them are goals relative to the current position of the robot like “move 3 meters right and then move 2 meters left”. Another one is an instruction with number reasoning like “move between the keyboard and the laptop twice”. We observe that failure cases are caused by: 1) inaccurate depth introduces noise during the map creation and decreases the landmark indexing accuracy 2) action noise can negatively influence the navigation performance at test time. Overall, these results demonstrate the ability of VLMaps to index landmarks with natural language in the real world and more importantly, its applicability to navigate to a wide variety of open-vocabulary language-based spatial goals.

V. DISCUSSION AND LIMITATIONS

In this work, we propose VLMaps, a spatial map representation enriched with pretrained visual-language features, which enables natural language indexing in the map. When combined with large language models, VLMaps can be applied in zero-shot spatial goal navigation and can be shared among multiple robots with different embodiments to generate new obstacles map in runtime. VLMaps is not without limitations. Notably, it remains sensitive to 3D reconstruction noise and odometry drift during navigation. It also cannot resolve object ambiguities during landmark indexing when the scene is cluttered with similar objects. In future work, we plan to improve VLMaps by using better visual language models and extending it to scenes with dynamic objects and moving humans.

REFERENCES

- [1] T. P. McNamara, J. K. Hardy, and S. C. Hirtle, "Subjective hierarchies in spatial memory." *Journal of Experimental Psychology: Learning, Memory, and Cognition*, vol. 15, no. 2, p. 211, 1989.
- [2] M. M. Chun and Y. Jiang, "Contextual cueing: Implicit learning and memory of visual context guides spatial attention," *Cognitive psychology*, vol. 36, no. 1, pp. 28–71, 1998.
- [3] E. L. Newman, J. B. Caplan, M. P. Kirschen, I. O. Korolev, R. Sekuler, and M. J. Kahana, "Learning your way around town: How virtual taxicab drivers learn to use both layout and landmark information," *Cognition*, vol. 104, no. 2, pp. 231–253, 2007.
- [4] S. Thrun, W. Burgard, and D. Fox, "A probabilistic approach to concurrent mapping and localization for mobile robots," *Autonomous Robots*, vol. 5, no. 3, pp. 253–271, 1998.
- [5] F. Endres, J. Hess, N. Engelhard, J. Sturm, D. Cremers, and W. Burgard, "An evaluation of the rgb-d slam system," in *2012 IEEE international conference on robotics and automation*. IEEE, 2012, pp. 1691–1696.
- [6] S. Tellex, T. Kollar, S. Dickerson, M. Walter, A. Banerjee, S. Teller, and N. Roy, "Understanding natural language commands for robotic navigation and mobile manipulation," in *Proceedings of the AAAI Conference on Artificial Intelligence*, vol. 25, no. 1, 2011, pp. 1507–1514.
- [7] M. MacMahon, B. Stankiewicz, and B. Kuipers, "Walk the talk: Connecting language, knowledge, and action in route instructions," *Def*, vol. 2, no. 6, p. 4, 2006.
- [8] P. Anderson, Q. Wu, D. Teney, J. Bruce, M. Johnson, N. Sünderhauf, I. Reid, S. Gould, and A. Van Den Hengel, "Vision-and-language navigation: Interpreting visually-grounded navigation instructions in real environments," in *Proceedings of the IEEE conference on computer vision and pattern recognition*, 2018, pp. 3674–3683.
- [9] P. Anderson, A. Shrivastava, J. Truong, A. Majumdar, D. Parikh, D. Batra, and S. Lee, "Sim-to-real transfer for vision-and-language navigation," in *Conference on Robot Learning*. PMLR, 2021, pp. 671–681.
- [10] A. Radford, J. W. Kim, C. Hallacy, A. Ramesh, G. Goh, S. Agarwal, G. Sastry, A. Askell, P. Mishkin, J. Clark *et al.*, "Learning transferable visual models from natural language supervision," in *International Conference on Machine Learning*. PMLR, 2021, pp. 8748–8763.
- [11] B. Li, K. Q. Weinberger, S. Belongie, V. Koltun, and R. Ranftl, "Language-driven semantic segmentation," in *International Conference on Learning Representations*, 2021.
- [12] S. Y. Gadre, M. Wortsman, G. Ilharco, L. Schmidt, and S. Song, "Clip on wheels: Zero-shot object navigation as object localization and exploration," *arXiv preprint arXiv:2203.10421*, 2022.
- [13] D. Shah, B. Osinski, B. Ichter, and S. Levine, "Lm-nav: Robotic navigation with large pre-trained models of language, vision, and action," *arXiv preprint arXiv:2207.04429*, 2022.
- [14] A. Zeng, A. Wong, S. Welker, K. Choromanski, F. Tombari, A. Purohit, M. Ryoo, V. Sindhwani, J. Lee, V. Vanhoucke *et al.*, "Socratic models: Composing zero-shot multimodal reasoning with language," *arXiv preprint arXiv:2204.00598*, 2022.
- [15] R. F. Salas-Moreno, R. A. Newcombe, H. Strasdat, P. H. Kelly, and A. J. Davison, "Slam++: Simultaneous localisation and mapping at the level of objects," in *Proceedings of the IEEE conference on computer vision and pattern recognition*, 2013, pp. 1352–1359.
- [16] J. McCormac, A. Handa, A. Davison, and S. Leutenegger, "Semanticfusion: Dense 3d semantic mapping with convolutional neural networks," in *2017 IEEE International Conference on Robotics and automation (ICRA)*. IEEE, 2017, pp. 4628–4635.
- [17] M. Runz, M. Buffier, and L. Agapito, "Maskfusion: Real-time recognition, tracking and reconstruction of multiple moving objects," in *2018 IEEE International Symposium on Mixed and Augmented Reality (ISMAR)*. IEEE, 2018, pp. 10–20.
- [18] J. McCormac, R. Clark, M. Bloesch, A. Davison, and S. Leutenegger, "Fusion++: Volumetric object-level slam," in *2018 international conference on 3D vision (3DV)*. IEEE, 2018, pp. 32–41.
- [19] B. Xu, W. Li, D. Tzoumanikas, M. Bloesch, A. Davison, and S. Leutenegger, "Mid-fusion: Octree-based object-level multi-instance dynamic slam," in *2019 International Conference on Robotics and Automation (ICRA)*. IEEE, 2019, pp. 5231–5237.
- [20] N. Hughes, Y. Chang, and L. Carlone, "Hydra: a real-time spatial perception system for 3d scene graph construction and optimization," *Proceedings of Robotics: Science and Systems. New York City, NY, USA, http://dx. doi. org/10.15607/RSS*, 2022.
- [21] S.-C. Wu, J. Wald, K. Tateno, N. Navab, and F. Tombari, "Scenegrphfusion: Incremental 3d scene graph prediction from rgb-d sequences," in *Proceedings of the IEEE/CVF Conference on Computer Vision and Pattern Recognition*, 2021, pp. 7515–7525.
- [22] J. Krantz, E. Wijmans, A. Majumdar, D. Batra, and S. Lee, "Beyond the nav-graph: Vision-and-language navigation in continuous environments," in *European Conference on Computer Vision*. Springer, 2020, pp. 104–120.
- [23] D. Fried, R. Hu, V. Cirik, A. Rohrbach, J. Andreas, L.-P. Morency, T. Berg-Kirkpatrick, K. Saenko, D. Klein, and T. Darrell, "Speaker-follower models for vision-and-language navigation," *Advances in Neural Information Processing Systems*, vol. 31, 2018.
- [24] P.-L. Guhur, M. Tapaswi, S. Chen, I. Laptev, and C. Schmid, "Airbert: In-domain pretraining for vision-and-language navigation," in *Proceedings of the IEEE/CVF International Conference on Computer Vision*, 2021, pp. 1634–1643.
- [25] J. Krantz, A. Gokaslan, D. Batra, S. Lee, and O. Maksymets, "Waypoint models for instruction-guided navigation in continuous environments," in *Proceedings of the IEEE/CVF International Conference on Computer Vision*, 2021, pp. 15 162–15 171.
- [26] Y. Hong, Z. Wang, Q. Wu, and S. Gould, "Bridging the gap between learning in discrete and continuous environments for vision-and-language navigation," in *Proceedings of the IEEE/CVF Conference on Computer Vision and Pattern Recognition*, 2022, pp. 15 439–15 449.
- [27] T. Brown, B. Mann, N. Ryder, M. Subbiah, J. D. Kaplan, P. Dhariwal, A. Neelakantan, P. Shyam, G. Sastry, A. Askell *et al.*, "Language models are few-shot learners," *Advances in neural information processing systems*, vol. 33, pp. 1877–1901, 2020.
- [28] A. Kamath, M. Singh, Y. LeCun, G. Synnaeve, I. Misra, and N. Carion, "Mdetr-modulated detection for end-to-end multi-modal understanding," in *Proceedings of the IEEE/CVF International Conference on Computer Vision*, 2021, pp. 1780–1790.
- [29] X. Gu, T.-Y. Lin, W. Kuo, and Y. Cui, "Open-vocabulary object detection via vision and language knowledge distillation," in *International Conference on Learning Representations*, 2021.
- [30] M. Shridhar, L. Manuelli, and D. Fox, "Cliport: What and where pathways for robotic manipulation," in *Conference on Robot Learning*. PMLR, 2022, pp. 894–906.
- [31] O. Mees, L. Hermann, E. Rosete-Beas, and W. Burgard, "Calvin: A benchmark for language-conditioned policy learning for long-horizon robot manipulation tasks," *IEEE Robotics and Automation Letters (RA-L)*, vol. 7, no. 3, pp. 7327–7334, 2022.
- [32] O. Mees, L. Hermann, and W. Burgard, "What matters in language conditioned robotic imitation learning over unstructured data," *IEEE Robotics and Automation Letters (RA-L)*, vol. 7, no. 4, pp. 11 205–11 212, 2022.
- [33] O. Mees, J. Borja-Diaz, and W. Burgard, "Grounding language with visual affordances over unstructured data," *arXiv preprint arXiv:2210.01911*, 2022.
- [34] B. Chen, F. Xia, B. Ichter, K. Rao, K. Gopalakrishnan, M. S. Ryoo, A. Stone, and D. Kappler, "Open-vocabulary queryable scene representations for real world planning," *arXiv preprint arXiv:2209.09874*, 2022.
- [35] M. Ahn, A. Brohan, N. Brown, Y. Chebotar, O. Cortes, B. David, C. Finn, K. Gopalakrishnan, K. Hausman, A. Herzog *et al.*, "Do as i can, not as i say: Grounding language in robotic affordances," *arXiv preprint arXiv:2204.01691*, 2022.
- [36] K. Zakka, A. Zeng, P. Florence, J. Tompson, J. Bohg, and D. Dwibedi, "Xirl: Cross-embodiment inverse reinforcement learning," in *Conference on Robot Learning*. PMLR, 2022, pp. 537–546.
- [37] A. Ganapathi, P. Florence, J. Varley, K. Burns, K. Goldberg, and A. Zeng, "Implicit kinematic policies: Unifying joint and cartesian action spaces in end-to-end robot learning," *arXiv preprint arXiv:2203.01983*, 2022.
- [38] J. Wu, X. Sun, A. Zeng, S. Song, S. Rusinkiewicz, and T. Funkhouser, "Spatial intention maps for multi-agent mobile manipulation," in *2021 IEEE International Conference on Robotics and Automation (ICRA)*. IEEE, 2021, pp. 8749–8756.
- [39] W. Huang, P. Abbeel, D. Pathak, and I. Mordatch, "Language models as zero-shot planners: Extracting actionable knowledge for embodied agents," *arXiv:2201.07207*, 2022.
- [40] W. Huang, F. Xia, T. Xiao, H. Chan, J. Liang, P. Florence, A. Zeng, J. Tompson, I. Mordatch, Y. Chebotar *et al.*, "Inner monologue: Embodied reasoning through planning with language models," *arXiv preprint arXiv:2207.05608*, 2022.
- [41] A. Zeng, "Learning visual affordances for robotic manipulation," Ph.D. dissertation, Princeton University, 2019.
- [42] J. Borja-Diaz, O. Mees, G. Kalweit, L. Hermann, J. Boedecker, and W. Burgard, "Affordance learning from play for sample-efficient policy learning," in *Proceedings of the IEEE International Conference on Robotics and Automation (ICRA)*, Philadelphia, USA, 2022.

- [43] J. Liang, W. Huang, F. Xia, P. Xu, K. Hausman, B. Ichter, P. Florence, and A. Zeng, "Code as policies: Language model programs for embodied control," *arXiv preprint arXiv:2209.07753*, 2022.
- [44] M. Chen, J. Tworek, H. Jun, Q. Yuan, H. P. d. O. Pinto, J. Kaplan, H. Edwards, Y. Burda, N. Joseph, G. Brockman *et al.*, "Evaluating large language models trained on code," *arXiv:2107.03374*, 2021.
- [45] M. Savva, A. Kadian, O. Maksymets, Y. Zhao, E. Wijmans, B. Jain, J. Straub, J. Liu, V. Koltun, J. Malik, D. Parikh, and D. Batra, "Habitat: A Platform for Embodied AI Research," in *Proceedings of the IEEE/CVF International Conference on Computer Vision (ICCV)*, 2019.
- [46] A. Chang, A. Dai, T. Funkhouser, M. Halber, M. Niessner, M. Savva, S. Song, A. Zeng, and Y. Zhang, "Matterport3D: Learning from RGB-D data in indoor environments," *International Conference on 3D Vision (3DV)*, 2017.
- [47] R. R. Selvaraju, M. Cogswell, A. Das, R. Vedantam, D. Parikh, and D. Batra, "Grad-cam: Visual explanations from deep networks via gradient-based localization," *International Journal of Computer Vision*, vol. 128, no. 2, pp. 336–359, 2020.
- [48] P. Anderson, A. Chang, D. S. Chaplot, A. Dosovitskiy, S. Gupta, V. Koltun, J. Kosecka, J. Malik, R. Mottaghi, M. Savva *et al.*, "On evaluation of embodied navigation agents," *arXiv preprint arXiv:1807.06757*, 2018.
- [49] M. Labbé and F. Michaud, "Rtab-map as an open-source lidar and visual simultaneous localization and mapping library for large-scale and long-term on-line operation," *Journal of Field Robotics*, vol. 36, no. 2, pp. 416–446, 2019.
- [50] J. Long, E. Shelhamer, and T. Darrell, "Fully convolutional networks for semantic segmentation," in *Proceedings of the IEEE conference on computer vision and pattern recognition*, 2015, pp. 3431–3440.

APPENDIX

A. Full List of Navigation Primitives

Our full list of navigation primitives are listed in Table IV.

primitives	functions
move_to(pos)	move to a position on the map.
move_to_left(object_name)	move to the left side of the nearest front object.
move_to_right(object_name)	move to the right side of the nearest front object.
get_pos(object_name)	get the map position of the nearest front object.
get_contour(object_name)	get the contour turning points of the nearest front object on the map.
with_object_on_left(object_name)	turn until the nearest object is on the robot's left side.
with_object_on_right(object_name)	turn until the nearest object is on the robot's right side.
move_in_between(object_a, object_b)	move in between two objects.
turn(angle)	turn right a certain angle. If the angle value is negative, turn left.
face(object_name)	turn until the nearest object is in front of the robot.
turn_absolute(angle)	turn to absolute angle. 0 is north, 90 is east, -90 is west, 180 is south.
move_north(object_name)	move to the north side of the nearest front object.
move_south(object_name)	move to the south side of the nearest front object.
move_east(object_name)	move to the east side of the nearest front object.
move_west(object_name)	move to the west side of the nearest front object.
move_to_object(object_name)	move to the nearest object.
move_forward(dist)	move forward "dist" meters.

TABLE IV: List of the navigation primitives used.

B. Full Prompts

Our full prompts used for getting the navigation results are listed below.

```
# move a bit to the right of the fridge
robot.move_to_right('refrigerator')
# move in between the couch and bookshelf
robot.move_in_between('couch', 'bookshelf')
# face the toilet
robot.face('toilet')
# move to the west of the chair
robot.move_west('chair')
# turn right 20 degrees
robot.turn(20)
# find any chairs in the environment
robot.move_to_object('chair')
# with the television on your left
robot.with_object_on_left('television')
# move forward for 3 meters
robot.move_forward(3)
# move right 2 meters
robot.turn(90)
robot.move_forward(2)
```

```
# move back and forth to the chair and table 3 times
pos1 = robot.get_pos('chair')
pos2 = robot.get_pos('table')
for i in range(3):
    robot.move_to(pos1)
    robot.move_to(pos2)
# move 3 meters south of the chair
robot.move_south('chair')
robot.face('chair')
robot.turn(180)
robot.move_forward(3)
# turn west
robot.turn_absolute(-90)
# turn east
robot.turn_absolute(90)
# turn south
robot.turn_absolute(180)
# turn north
robot.turn_absolute(0)
# turn east and then turn left 90 degrees
robot.turn_absolute(90)
robot.turn(-90)
# navigate to 3 meters right of the table
robot.move_to_right('table')
robot.face('table')
robot.turn(180)
robot.move_forward(3)
```

C. Prompt engineering.

For all methods in this work (including baselines), when using CLIP text encoding, instead of simply prompting the label of the object categories, we use the ensemble of prompt templates like "A photo of label", "A picture of label" mentioned in [10] to improve the retrieval performance.

D. Top-Down Map Semantic Segmentation

For ablation purposes, we compute the semantic segmentation masks for the top-down maps in the Habitat simulator with the Matterport3D dataset. We use the collected RGB-D frames mentioned in Sec. IV-A to create the VLMaps and the CLIP on Wheels saliency maps. We evaluate all the semantic categories (the full list can be found in the link¹) supported in the Matterport3D dataset except "void", "floor", "ceiling", "objects", "misc". To get the ground truth semantic masks, we use the RGB-D frames and the ground truth image semantic masks to create a semantic top-down map. We back-project the depth pixels to the 3D space and project them to the top-down map. We assign the associated semantic values to the top-down map pixels. If multiple points are projected to the same location, we overwrite the old value if the new point's height is larger than the previous points. To compute semantic masks for VLMaps, we apply the open-vocabulary landmark indexing technique described in Sec. III-B to the whole list of categories. To compute semantic masks for the CLIP on Wheels, we compute the saliency values and apply the same thresholding process as in [12] to get a binary mask for each category. We evaluate the semantic segmentation metrics used in [50]. The segmentation results is shown in Table V.

We also show the IOU values of the top-10 frequent categories in Table VI. The table shows that VLMaps performs better than

¹<https://github.com/niessner/Matterport/blob/master/metadata/mpcat40.tsv>

CoW Map in most of the top-10 frequent categories. This is mainly because the GradCam used in CoW introduces a lot of noise in the saliency map, causing over-segmentation in the results. We also note that in the class “seating”, VLMaps gets 0 IOU score. Since the LSeg model we used is pre-trained on segmentation datasets where some query classes might not be in the pre-defined training categories, LSeg’s visual encoder will encode visually unseen objects (“seating”) to a similar seen object’s embedding space (like “chair” or “sofa” here). As a result, visual-text misalignment could happen.

Metric	CoW Map	VLMaps (ours)
pixel accuracy	66.1	92.3
mean accuracy	9.6	27.7
mIOU	5.7	19.0
frequency weighted mIOU	42.9	85.9

TABLE V: Top-Down Map Semantic Segmentation Results.

Class	Class Portion	IOU	
		CoW	VLMaps (ours)
wall	39.70	63.80	98.57
chair	9.66	6.99	77.04
table	8.14	1.20	13.82
door	4.94	12.50	28.28
seating	4.54	8.77	0.00
stairs	3.75	12.35	22.02
cabinet	3.38	1.13	1.87
sofa	2.7	1.66	24.46
bed	2.64	2.47	38.3
shelving	2.60	0.87	1.59

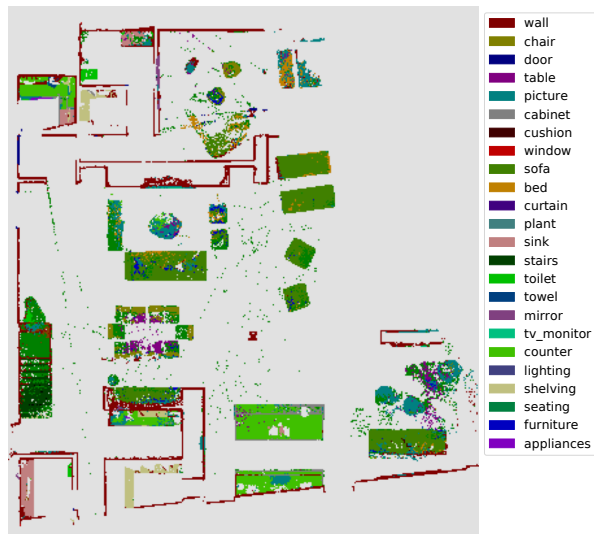
TABLE VI: Top-10 frequent per-class IOU

We visualize qualitative segmentation results in Figure 6. We observe that for categories “wall”, “chair”, “counter”, “table”, and “bed”, the segmentation results are mostly correct. Sometimes, when the “sofa” and “chair” are in similar material and shape (in Figure 6a and 6b), VLMaps might fail to differentiate them, leading to wrong planning behaviors. We also observe from Figure 6c and Figure 6e that the segmentation of some objects are noisy. This could be caused by the features fusion strategy we adopt. For example, in the top left corner of Figure 6e, there are some chairs and tables predictions with noise compared to the ground truth in Figure 6f. When we generate VLMaps for the scenes, we average the visual embeddings of points projecting to the same location on the top-down map. The averaging operation might introduce noise in the fused features, leading to noisy segmentation predictions (predicting “sink” on the table). In the future, more advanced fusion techniques can be explored to improve the segmentation results.

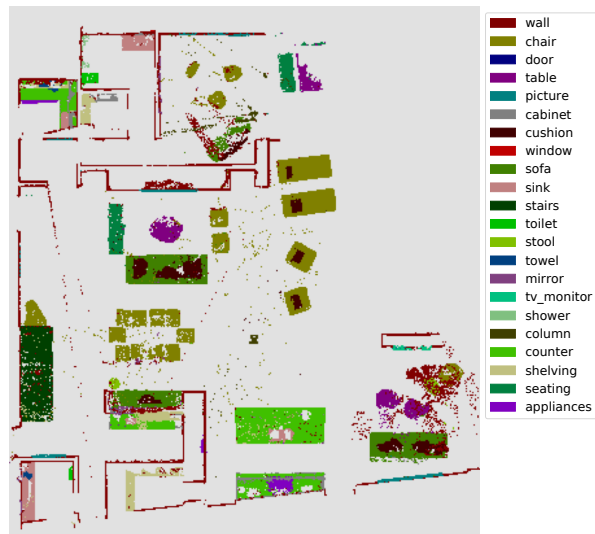
E. Prompts for Obstacle Maps Generation

In Sec. IV-D, we generate open-vocabulary obstacle maps for a drone and a LoCoBot with the method introduced in Sec. III-C. For the LoCoBot (ground robot), we first define a potential obstacle list as [“chair”, “wall”, “wall above the door”, “table”, “window”, “floor”, “stairs”, “other”] and perform open-vocabulary landmark indexing. Later, we only select the union of the masks for the objects “wall”, “chair”, “table”, “window”, “stairs”, “other”

as the obstacle map. For the drone (flying robot), we perform landmark indexing with the potential obstacle list: [“chair”, “sofa”, “wall”, “table”, “counter”, “window”, “floor”, “stairs”, “ceiling lights”, “cabinet”, “counter support”, “other”]. Afterwards, we take union of the masks for [“wall”, “window”, “stairs”, “ceiling lights”, “cabinet”, “other”] to generate the obstacle map.



(a) VLMs (sequence 1)



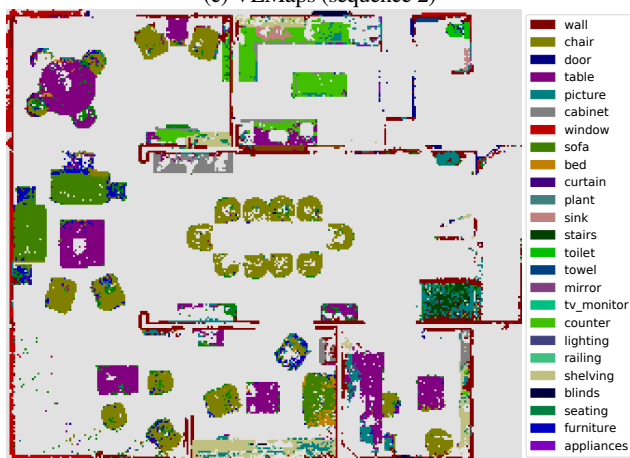
(b) GT (sequence 1)



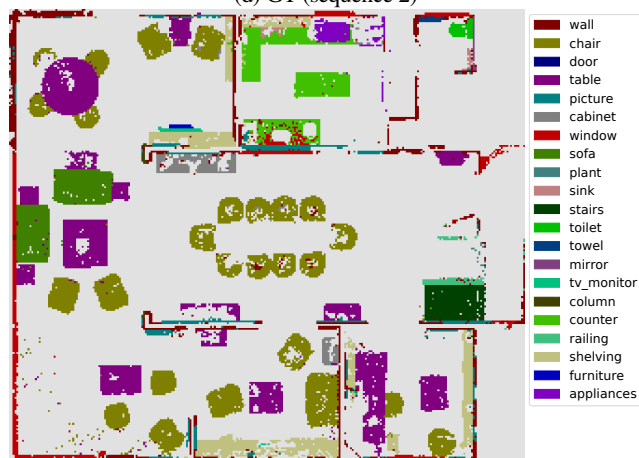
(c) VLMs (sequence 2)



(d) GT (sequence 2)



(e) VLMs (sequence 3)



(f) GT (sequence 3)

Fig. 6: Qualitative semantic segmentation results